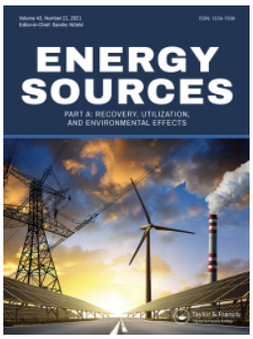

Taylor & Francis
Taylor & Francis Group

Energy Sources, Part A: Recovery, Utilization, and Environmental Effects

ISSN: 1556-7036 (Print) 1556-7230 (Online) Journal homepage: www.tandfonline.com/journals/ueso20

An image encryption concept based solar photovoltaic array reconfiguration techniques for mismatch mitigation

Rayappa David Amar Raj & Kanasottu Anil Naik

To cite this article: Rayappa David Amar Raj & Kanasottu Anil Naik (2022) An image encryption concept based solar photovoltaic array reconfiguration techniques for mismatch mitigation, Energy Sources, Part A: Recovery, Utilization, and Environmental Effects, 44:1, 951-972, DOI: 10.1080/15567036.2022.2052383

To link to this article: https://doi.org/10.1080/15567036.2022.2052383

ENERGY SOURCES, PART A: RECOVERY, UTILIZATION, AND ENVIRONMENTAL EFFECTS
2022, VOL. 44, NO. 1, 951–972
https://doi.org/10.1080/15567036.2022.2052383

An image encryption concept based solar photovoltaic array reconfiguration techniques for mismatch mitigation

Rayappa David Amar Raj and Kanasottu Anil Naik

Department of Electrical Engineering, National Institute of Technology, Warangal, India

ABSTRACT

The partial shading phenomenon significantly limits the PV array output. To maximize the output power during shading, various reconfiguration techniques have been reported in the literature. However, many of these techniques are not scalable, ineffective, and inconsistent in uniform shade dispersion. Therefore, two highly efficient Arnold's Cat Map and Henon Map-based chaotic approaches which are widely used in image encryption are employed to effectively disperse the shade by reconfiguring the modules without disturbing the electrical circuitry. The proposed approaches are evaluated in a MATLAB environment for symmetrical 8 × 8 PV array and unsymmetrical 5 × 7 PV array under different groups of progressive shading like left-to-right, triangular, top-to-bottom, and diagonal shading conditions. The efficacy of the proposed approaches is compared with conventional Series-Parallel, Total-Cross-Tied, existing Chaotic Baker-Map, Odd-Even, and Odd-Even-Prime-based reconfiguration techniques and extensively analyzed using different performance indices. A laboratory experimental setup of a 4 × 4 PV array reconfiguration system is developed and examined under distinct progressive shading cases. From the quantitative results obtained, it is noted that the proposed approaches offer consistently superior and reliable performance compared to existing state-of-art configurations under shading reinforcing their effectiveness.

ARTICLE HISTORY
Received 30 November 2021
Revised 3 March 2022
Accepted 4 March 2022

KEYWORDS
Arnold's Cat Map; Henon map; global maximum power; partial shading; reconfiguration

Introduction

The PV panels are inevitably subjected to shadowing issues due to large buildings, accretion of dust, bird shit on the panels, passing clouds, long trees, long poles, overhead transmission wire lines, etc. (Ahmad et al. 2017). During partial shading (PS), the temperature in the shaded cells raises and leads to the formation of hotspots which further leads to fire hazards and eventually devastates the panel. The damaged, faulty panels and corroded electrical connections lead to abnormal temperature diffusion. Early identification of hotspots and faults using proper characterization strategies could improve PV panel lifespan. Visual examination, Infrared thermography, and Ultraviolet Fluorescence imaging are the potential and mostly employed tools for fault diagnosis (Rahman, Khan, and Alameh 2021). Due to the booming implementation of deep-learning in pattern recognition and image processing, the thermal imaging-based methods integrated with AI and IoT-based approaches (Mellit and Kalogirou 2021) are gaining more popularity for detecting various faults in PV farms. Regardless, the distance between PV array, IR cameras, drones, and resolution must be considered to improve image quality, which aids in accurate fault diagnosis. Hotspots can be avoided by installing the bypass diodes across the panels. These diodes bypass the current under low irradiation conditions. Nevertheless, these diodes lead to multiple peaks in the array characteristics and also reduce the output (Celikel, Yilmaz, and Gundogdu 2022). To track the global maximum power (GMP), the modules in

CONTACT Rayappa David Amar Raj dtcdavid2k15@gmail.com Department of Electrical Engineering , National Institute of Technology, Warangal, India

an array are installed with MPPT controllers (Celikel, Yilmaz, and Gundogdu 2022). Despite its better technical performance, employing these controllers requires complex power converters and control algorithms making the system cost-ineffective. Further, to extract maximum output beyond what is solely achieved by MPPT alone, the reconfiguration techniques (Belhachat and Larbes 2021) are employed.

The reconfiguration techniques are classified as static and dynamic reconfiguration techniques. The literature review of some notable dynamic reconfiguration techniques is as follows: A dynamic auto-reconfiguration technique was experimentally investigated in Pachauri et al. (2019) on a 3 × 3 PV array under continuous shading conditions employing numerous arduino based relays. An efficient reconfiguration approach employing image processing-based shadow detection and optimization is proposed in Karakose et al. (2016). Image processing is used to obtain shadow information and a clonal selection method is selected for optimization. Despite its effectiveness, this approach needs switching matrices, complex algorithms, camera to monitor shading, and other accessories. To narrow down the row current variation and to reduce the multiple local maximum power peaks (MPPs) in array characteristics, various population-based metaheuristic algorithms such as genetic algorithm, GA (Deshkar et al. 2015), particle swarm optimization, PSO (Babu et al. 2018), modified harries hawk, MHH (Yousri, Allam, and Eteiba 2020) are proposed. In these approaches, the physical position of panels remains fixed, while the electrical circuitry is changed. In (Babu, Yousri, and Balasubramanian 2020), various three distinct population-based optimization algorithms are employed for switching matrices to reconfigure the PV array dynamically. By employing these techniques, there is an enhancement in GMP by 13%. Nevertheless, employing these optimization algorithms spur numerous challenges and complications such as convergence issues, difficulty in selection of optimal tuning parameters, problems associated with weighted sum approach, assignment of improper weights affecting the output, complex search mechanisms, etc. and further need numerous sensors and switches for operation.

Very recently, a new voltage equalization approach based on the hybridization of TCT arrangement and switching capacitor (TCT-SC) concept which uses the charge balancing concept is proposed for improving the power output during shading (Satpathy et al. 2021). To enhance the reliability of a PV array that is exposed to frequent shading conditions, a novel algorithm is proposed in Yadav et al. (2022) to limit the reverse current through a shaded module by mitigating the reverse voltage across the module. Nevertheless, this approach involves numerous switches and substantial solid-state switching device losses. The dynamic reconfiguration techniques enhance the output by mitigating the mismatch losses during shading, however they involve numerous complicated switches, complex algorithms to operate these switches, complex controlling units, efficient driver circuits, sensors, systematic monitoring units, composite wiring which makes the system totally complicated and uneconomical. In Ajmal et al. (2021), it is reported that the number of switches required to dynamically reconfigure a 9 × 9 PV array is 1384.

The static array reconfiguration schemes are regarded as a best alternative as they completely eliminate the above-mentioned challenges and some of the notable schemes are listed as follows: The authors proposed a reconfiguration approach based on sudoku (Rani, Ilango, and Nagamani 2013) puzzle to dispense the shading in the array to reduce the shading losses thereby increasing the global maximum power. Nevertheless, this technique fails to disseminate the shade in first column and hence the effectiveness of shading dispersal is reduced as it is not dispersed over the entire array. An improvised version of the sudoku puzzle named modified sudoku puzzle pattern (Rajani and Ramesh 2021) is recently proposed to reconfigure the panels. To obtain the single peak in array characteristic which allows the GMP tracking with simple controlling eliminating the demand for complicated control algorithms and expensive hardware, three shifted PV array configurations are proposed (Belhaouas et al. 2017). Nevertheless, these configurations under perform under diagonal shading conditions. A fixed electrical reconfiguration technique (Satpathy and Sharma 2019) that employs a novel algorithm to renumber the PV panels in an array is proposed to disperse the shade for alleviating the mismatch losses. A Lo shu magic square-based array reconfiguration technique is

proposed in Venkateswari and Rajasekar (2020) for a 9 × 9 PV array for effective shade dispersal. However, the major drawback of this configuration is that it cannot be implemented for the PV arrays of sizing other than 9 × 9. To obtain the equal row irradiance, the authors in Pachauri et al. (2018) proposed a new Latin square reconfiguration strategy for a 4 × 4 PV array. This technique effectively disperses the shade under left-to-right, bottom-to-top, zigzag, and diagonal shading conditions. But the authors fail to prove the feasibility of the proposed algorithm for a large rated PV system.

A puzzle-based dominance square method is proposed for a 5 × 5 PV array to physically relocate the panels in a row and column-wise manner (Dhanalakshmi and Rajasekar 2018). However, this technique is highly ineffective under diagonal shading conditions. In Yadav, Pachauri, and Chauhan (2016), a ken ken squared puzzle-based reconfiguration technique is verified on 6 × 6 PV array to relocate the PV modules in order to minimize the shading effects on the output. Majority of these puzzle-based techniques are not compatible with all the array sizes and hence they cannot be generalized. Besides, many of these techniques fail to disperse the shade over the entire PV array. To mitigate the multiple power in the array characteristics under shading, a fixed shade dispersion positioning (SDP) strategy is proposed for 3 × 3 and 5 × 5 PV arrays without altering the electrical connections (Satpathy and Sharma 2018). Recently, a novel magic square (MS) approach is proposed for minimizing the row current variation in an array by physical relocation (Varma, Barry, and Jain 2021). The output is enhanced by 11.53%, however, the application of MS-based techniques is highly limited as it is not compatible with all array sizes. To disperse the shade of the PV array irrespective of its size, a shade distribution process that takes place in two distinct phases has been implemented in Pillai et al. (2018) for a 9 × 9 array. However, the results showed that the efficacy of this technique under short and narrow shading pattern type is inadequate. In Horoufiany and Ghandehari (2018), a new optimized reconfiguration technique has been employed to lessen the effects of mutual shading irrespective of the shading factors like the sun's position, system's latitude, and the installation aspects of the PV by displacing the PV modules in a TCT configuration without remodeling the electrical circuitry.

In Tatabhatla, Agarwal, and Kanumuri (2020), a new image processing-based PV array reconfiguration technique inspired by the Chaotic Baker's Map (CBM) has been proposed for an 8 × 8 PV array. By exercising this technique, the PV array row currents mismatch is mitigated and yields superior performance when compared to conventional array configurations under all the shading conditions. Despite its better performance with respect to conventional configurations, the CBM technique inherits the following major drawbacks: ineffective shade dispersion over the entire array and inapplicability for unsymmetrical PV arrays. A uniform shade dispersion by physical relocation of panels is performed by the SD-PAR strategy (Satpathy, Sharma, and Dash 2019). The effectiveness of this technique is compared with the conventional configurations and also the existing EAR technique. A sensorless fixed array configuration based on Knight's tour pattern is proposed to mitigate mismatch losses (Rezazadeh et al. 2022). But finding the optimal arrangement is quite challenging as there exist numerous solution sets for this technique. A simple approach named sequential arrangement technique (Rakesh et al. 2022) is recently proposed for a 3 × 3 array. The effectiveness of this technique has not been verified for the large-rated PV arrays. Moreover, the highest power enhancement is evidently only 12%. A computer algorithm-based optimal interconnection scheme (Satpathy, Sharma, and Jena 2017) for PV panels is proposed and experimented on a 3 × 3 and 7 × 7 PV array to disperse the shade evenly thereby minimizing the shading loss. An odd-even (OE) (Nasiruddin et al. 2019) and odd-even-prime (OEP) (Reddy and Yammani 2020) ordering-based physical redeployment of the PV modules has been introduced to alleviate the shading losses. However, these techniques despite being compatible exhibit poor shading dispersal maximizing the mismatch losses. The applicability of image encryption-based chaotic mapping techniques for reconfiguring the PV array is not explored by the researchers. The major objectives and research gaps identified in the literature are as follows:

- Most of static reconfiguration techniques are not applicable for both symmetrical and nonsymmetrical size of PV arrays.
- Need for effective and even shade dispersion scheme over the entire array.

- A majority of techniques despite exhibiting better performance under some cases fail to be effective under other cases resulting in inconsistent performance. Moreover, under some shading conditions, they produce lower output compared to conventional configurations.
- Analysis with real-time progressive and dynamic shading conditions (due to moving clouds, moving shade of neighboring buildings, long towers, poles, etc.) over PV array is hardly explored in literature.
- Some techniques despite enhancing the output exhibit numerous MPPs (due to uneven dispersion) in the array characteristics. This necessitates complex and sophisticated MPPT controllers to differentiate between global and local maxima to extract the maximum attainable energy with an imposed burden on them.
- Employment of image encryption techniques for dispersing the shade through reconfiguration is hardly explored in the literature.

The present research work addresses all the above-mentioned concerns in the subsequent sections. The novelty and major contributions of the proposed work:

- For the first time, three highly efficient, simple, sensorless chaotic map-based PV array reconfiguration approaches are proposed to effectively disperse the shade.
- On contrary to numerous existing static reconfiguration techniques, the proposed ones are compatible for any array sizes such as 5×5, 7×9, 23×17, etc. For analysis, distinct symmetrical and unsymmetrical PV array sizes such as 4×4, 8×8, and 5×7 are considered.
- As opposed to many static reconfiguration techniques that indiscriminately disperse the shade, the proposed techniques intelligently disperse the shade. This is achieved by the chaotic approaches where the correlation between the adjacent shaded modules in a row is reduced significantly thereby improving the total irradiation of a particular row of PV array.
- For practical realization, the proposed configurations are experimented with under distinct realistic progressive shading and moving shade conditions.
- The significant reduction in MPPs and the smoother characteristics obtained by the proposed techniques make the GMP tracking simple, less complex, and cost-effective.
- A laboratory experimental setup of a 4×4 PV array reconfiguration system is developed and examined under distinct progressive and moving shade conditions.

Modeling of solar cell

The PV cell modeling is a crucial aspect in determining the performance efficiency of an array. Several approaches for modeling a PV cell are published in the literature as follows: one diode model, two diodes model, and three diodes model. The two-diode and three-diode models lead to a more accurate solution as they consider the recombination loss (Ndi et al. 2021). However, they require powerful and robust algorithms to extract the unknown parameters to acquire better accuracy. Further, the three-diode model has not been examined considerably due to its calculation complexity. Including an extra diode, nevertheless, raises the unknown parameters to be computed, complexity, computational time, and computing burden. Hence a one-diode model (from Figure 1) is used for modeling in this work which also achieves acceptable accuracy.

By employing KCL at the junction 'N,' the PV cell output current (I) is obtained as follows,

$$I = I_{Ph} - I_0 \times \left[\exp\left(\frac{V_D}{\alpha V_T}\right) - 1\right] - \frac{V_{PV} + IR_s}{R_{sh}} \tag{1}$$

where 'I_{Ph}' is the photon-current generated, 'I_D' is the diode current, 'R_s' is the series resistor, 'R_{sh}' is the shunt resistor 'V_{PV}' is the cell voltage and 'I' is the cell current, 'I_o' is the Module reverse saturation current, 'α' is the ideality factor of diode D and 'V_T' is the thermal voltage.

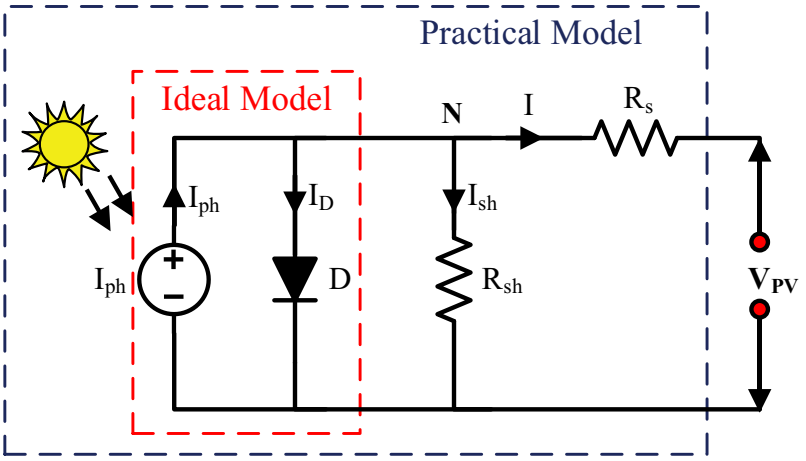

Figure 1. A one diode equivalent circuit model.

Proposed methodology

The proposed methodology is based on widely employed chaotic map approach-based techniques in the field of image encryption which are discussed as follows.

Image encryption based on chaotic mapping approach

In image encryption, an image is regarded to be constituted of pixels and when it is operated with a transformation, the original position of its pixels is randomly relocated (Shahna and Mohamed 2020). The digital image is regarded to be a two-dimensional m × n matrix, where m and n indicate the respective number of rows and columns of an image. To intensify security, the image is encrypted by transforming the pixel locations in an image. The location of the pixel is transformed based on the secret-key algorithm which can be decoded by the end-users only. Various chaotic maps are the commonly exercised tools for encrypting an image. In this paper, a well-regarded 2D Arnold's cat map (Li et al. 2022) and 2D Henon map (Peng, Sun, and He 2020) based chaotic approaches which are widely used in the encryption process are employed for reconfiguring the PV array under shading. Generally, the two-dimensional chaotic maps are represented as follows:

$$\left.\begin{aligned} x_{i+1} &= r(x_i, y_i) \\ y_{i+1} &= s(x_i, y_i) \end{aligned}\right\} \tag{2}$$

where x, y are the matrix coordinates and 'r,' 's' are two given functions. Figure 2 shows the original image of solar-powered home and its corresponding encrypted image obtained by Arnold's Cat Map algorithm. From the figure it is noted that the pixels in the original image are scrambled very effectively for better security purpose.

A two-dimensional arnold's cat map

A 2D Arnold's Cat Map (ACM) is a discrete system that provides a chaotic behavior which was developed by a Russian mathematician Vladimir I. Arnold in 1960. This was experimented with by using an image of a cat, and hence the title Arnold's cat map (Li et al. 2022). The representation of Arnold's Cat Map equation is described as follows

Figure 2. Original image of solar-powered home and its corresponding encrypted image.

$$\begin{pmatrix} x_{i+1} \\ y_{i+1} \end{pmatrix} = \begin{pmatrix} 1 & 1 \\ 1 & 2 \end{pmatrix} * \begin{pmatrix} x_i \\ y_i \end{pmatrix} mod1 \tag{2}$$

Further, the map can be generalized (Li et al. 2022) as follows:

$$\begin{pmatrix} x_{i+1} \\ y_{i+1} \end{pmatrix} = \begin{pmatrix} 1 & a \\ b & ab+1 \end{pmatrix} * \begin{pmatrix} x_i \\ y_i \end{pmatrix} modN \tag{3}$$

where x_i and y_i are the old pixel locations and, x_{i+1} & y_{i+1} are the new pixel locations. In Eq. (4), 'a' and 'b' are the system control parameters and 'N' indicates the size of the image that is to be encrypted. By using ACM algorithm, the old pixel locations (x_i, y_i) are transformed to new pixel locations (x_{i+1}, y_{i+1}) as shown in Figure 4.

A two-dimensional henon map

A 2D Henon Map (HM) is a two-dimensional discrete time dynamical system that was presented by Michel Henon as a demonstration model for a Lorenz model (Peng, Sun, and He 2020). A classical 2D Henon map has discrete time, however, the state variables (x, y) are continuous. The general mathematical equation of Henon Map (Peng, Sun, and He 2020) is described as follows:

$$\left.\begin{aligned} x_{i+1} &= \left(1 + y_i - ax_i^2\right) modN, \\ y_{i+1} &= (bx_i) modN \end{aligned}\right\} \tag{5}$$

To expedite the discrete digital image processing, a discrete Henon map (Ping et al. 2015) is represented as

$$\left.\begin{aligned} x_{i+1} &= \left(1 - ax_i^2 + y_i\right) modN \\ y_{i+1} &= (x_i + c) modN \end{aligned}\right\} \tag{6}$$

where x, y are the state variables, x_i, y_i are the old pixel locations and, x_{i+1}, y_{i+1} are the new pixel locations, a and b are the control parameters, 'i' is the number of iterations, 'N' is the order of digital image. By using the respective ACM and HM algorithms, the original coordinates (x_i, y_i) of the matrix are scrambled to form the rearranged coordinates of the matrix according to the equations given from Eq. (3) to (6). Figure 3 shows the image encryption process and generalized pseudocode of the ACM and HM techniques for rearranging the matrix elements. The numbers 1 to 9 are placed in a row-wise manner in a 3 × 3 matrix. By applying a chaotic map, the numbers are scrambled as shown in Figure 3 (b). Based on the obtained rearranged matrix by a chaotic map approach, the pixel coordinates of the original matrix are transformed to new pixel coordinates. For example, the number '5' of rearranged

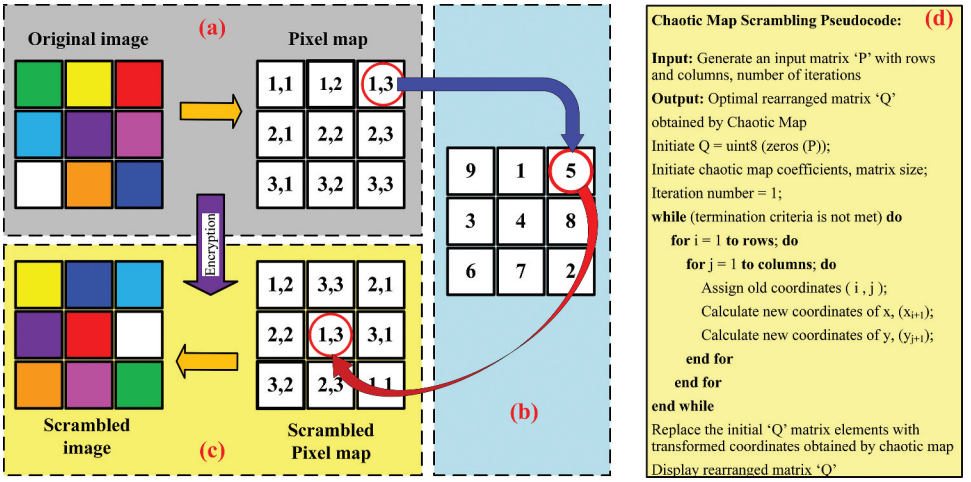

Figure 3. Image encryption process (a) Original image (b) rearranged matrix (c) scrambled image (d) Generalized pseudocode of the proposed ACM and HM techniques.

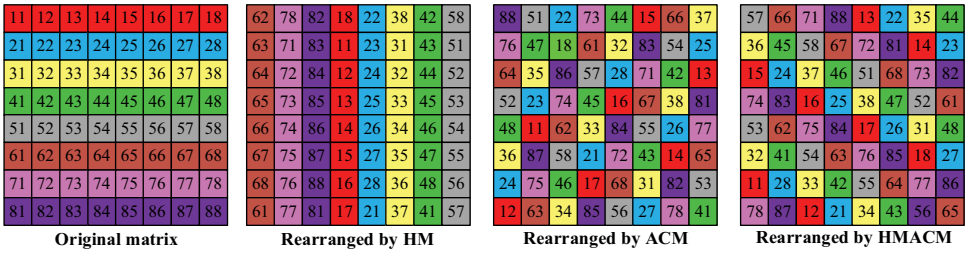

Figure 4. Original matrix and the respective reconfigured matrix obtained by HM, ACM and HMACM approaches.

matrix is located in (1,3) coordinates. So, based on this rearranged matrix, the corresponding pixel coordinate (1,3) of the original image which is in red color is now moved to the second row and second column (2,2) coordinate of the new matrix.

A two dimensional dual-stage chaotic map

In addition to the above-mentioned approaches, a dual-stage chaotic map approach named Henon Map-Arnold's Cat Map (HMACM) is proposed. This is obtained by applying both HM and ACM chaotic maps in subsequent stages to attain a much better scrambling which further reduces the correlation between the adjacent pixels. In this approach, elements of the matrix are scrambled by using Eq. (6) of HM approach, and then the ACM algorithm is applied to the rearranged matrix (obtained by HM approach) by using Eq. (4). Due to the application of two chaotic map approaches subsequently, the elements in the matrix got more effectively rearranged with reduced correlation coefficient compared to both ACM and HM approaches as reflected in Figure 4 and hence it can be also employed to optimally configure the PV array.

Reconfiguration using ACM, HM and dual-stage HMACM chaotic approaches

The central aim of image encryption is to decrease the correlation between adjacent pixels in an image (Shahna and Mohamed 2020). The encryption concept is employed here by considering the individual PV module as a pixel of image, and these modules are reconfigured intelligently for distributing the shade over the PV array. With the employment of this image encryption concept in the reconfiguration process, the

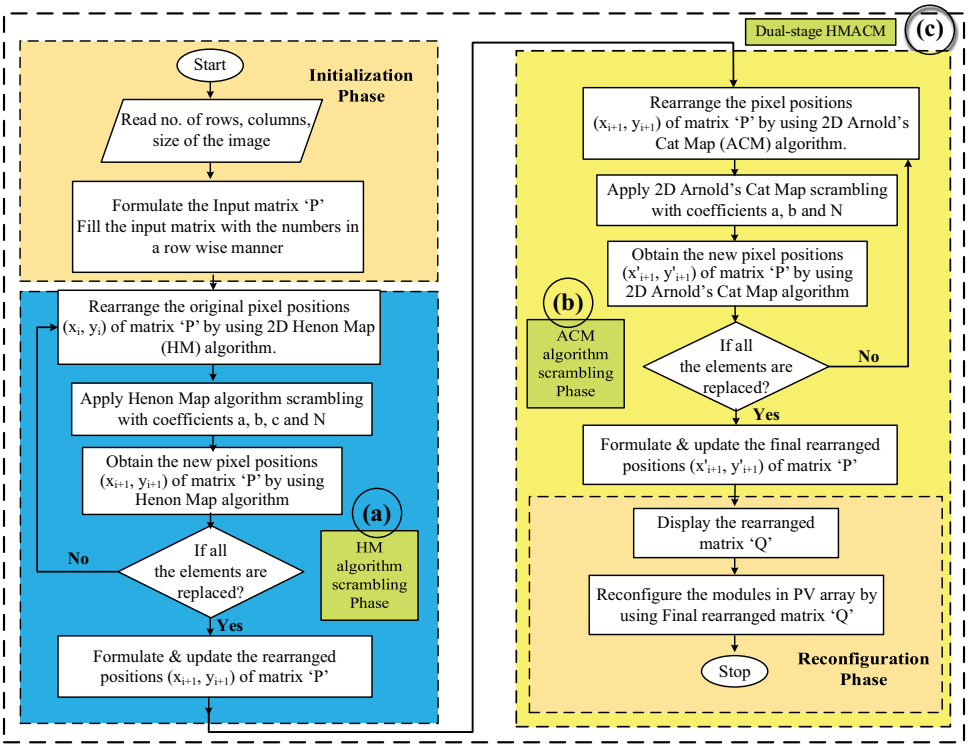

Figure 5. Flowchart of PV array reconfiguration technique describing (a) HM scrambling phase (b) ACM scrambling phase and (c) Dual-stage HMACM scrambling.

correlation between the adjacent shaded modules in a particular row is highly reduced thereby enhancing the total irradiation of the row of a PV array. The PV array is effectively reconfigured by relocating the panels based on the optimal pattern of HM, ACM, and HMACM matrices without altering the electrical circuitry. This does not evoke any variations in its electrical properties and further lessens the shading intensity by dispersing the shade over the PV array. The evolution of the proposed ACM reconfiguration scheme is shown in Figure 6. For instance, the PV panel '23' is electrically and physically connected between node 'B' and 'C' in TCT configuration as shown in Figure 6. After reconfiguration with the ACM approach, it is moved to the fourth row and second column i.e., between node 'D' and 'E' while it is electrically connected between node 'B' and 'C.' Similarly, all the panels are configured based on the obtained ACM matrix. So, if the shade occurs in any part of array, it is dispersed in all rows and columns uniformly by the proposed image encryption-based PV array reconfiguration strategies maximizing energy yield. The detailed flowchart of the proposed technique for reconfiguring the PV array is shown in Figure 5.

Performance indices

The following parameters are considered to evaluate the efficacy of the proposed techniques.

Global maximum power (GMP)

It is the maximum power output that can be extracted from the PV array.

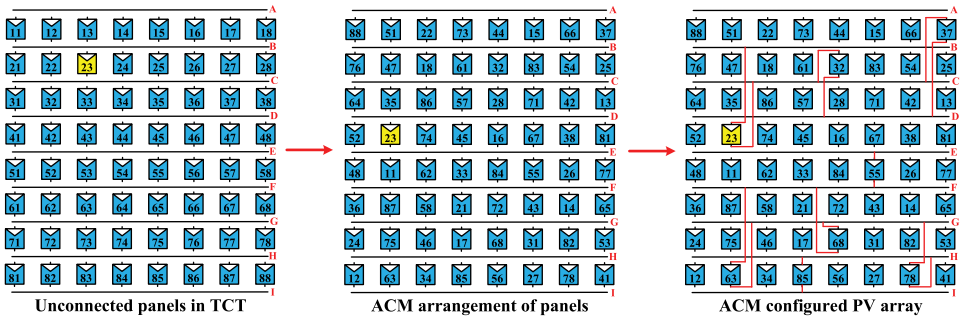

Figure 6. Evolution and development of ACM configured PV array from the conventional TCT configuration.

Mismatch power (MM_P)

Mismatch power losses occur due to the connection of PV modules having distinct characteristics (Smith, Matam, and Seigneur 2021). It is the difference between GMP obtained at unshaded (GMP_{STC}) and the GMP obtained at shaded conditions (GMP_{PS}).

$$MM_P(W) = GMP_{STC} - GMP_{PS}$$

Fill factor (FF)

Fill Factor is the ratio of the maximum power (P_{max}) to the product of V_{oc} and I_{sc} of the PV cell. Higher the FF value, the obtained IV characteristics are close to the square shape. FF is determined as follows:

$$FF = \frac{V_{mpp} \times I_{mpp}}{V_{oc} \times I_{sc}} = \frac{P_{max}}{V_{oc} \times I_{sc}}$$

Results and discussion

The conventional TCT, existing CBM (Tatabhatla, Agarwal, and Kanumuri 2020) and the proposed ACM, HM, and HMACM configurations are analyzed and tested for a 11.5 kW, 8 × 8 PV array (with nominal voltage and current at P_{max} are 195.51 V and 59.24 A, overall efficiency of 14.26%) in MATLAB under various shading cases of distinct shading groups such as progressive top-to-bottom, triangular, left-to-right, and diagonal shading patterns. The primary occurrences of these shadings are neighboring panels, tall and nearby buildings, moving clouds, elevated poles, towers, chimneys, roof ornaments, etc., whose density increases as it progresses. The advantage of these shading cases is that they can act as dynamic and static shades when held as individual shading cases. A Kyocera KG200GT PV panel is considered for the analysis. To validate the superiority of the proposed configurations, the system is examined by the aforementioned performance indices. For simulation studies and analysis, the unshaded and shaded modules are considered to receive 900 W/m^2 and 200 W/m^2 respectively.

During progressive left-to-right shading

During the progressive left-to-right shading condition, a group of three distinguished shading patterns of case-1 to case-3 is considered to be dynamically moving from left side to right side of the PV array as shown in Figure 7.

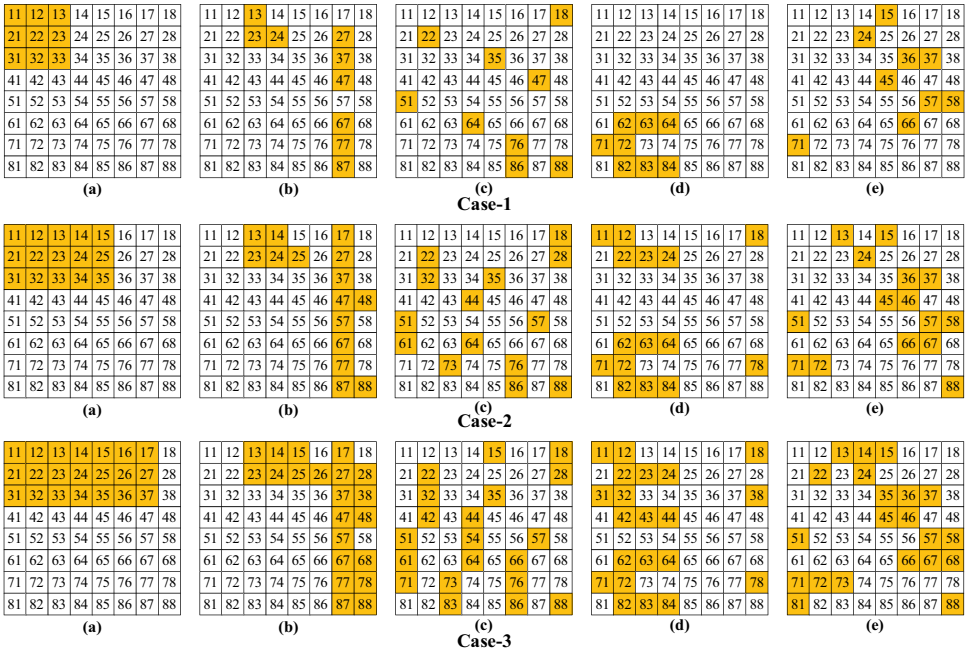

Figure 7. Progressive left-to-right shading in (a) TCT, shade dispersion with (b) CBM (c) ACM (d) HM and (e) HMACM for case-1, case-2 and case-3 respectively.

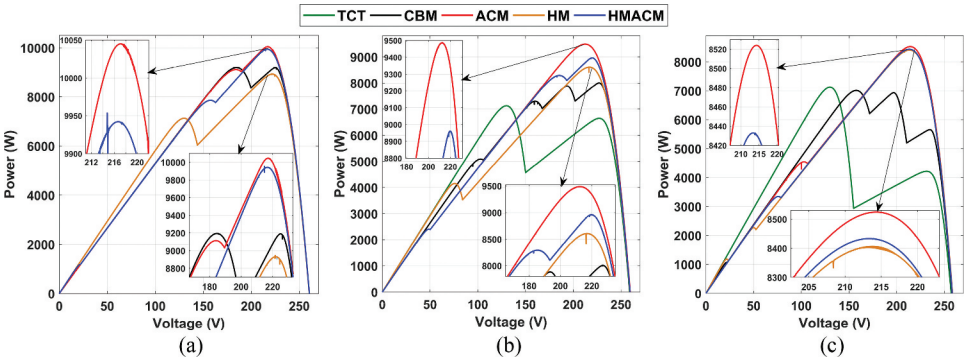

Figure 8. PV characteristics under progressive left-to-right shading of (a) case-1 (b) case-2 and (c) case-3.

From the PV characteristics of TCT, CBM, ACM, HM, and HMACM configurations shown in Figure 8, it is observed that the proposed ACM and HMACM configurations exhibit very fewer MPPs compared to all other configurations and hence smoother PV array characteristics are obtained. Under the three cases, the GMP obtained by TCT configuration is very low.

During the case-1 shading pattern, the GMP obtained by the proposed ACM and HMACM configurations is significantly enhanced by 12.43% and 11.4% compared to that of TCT and when compared to the CBM configuration, the GMP obtained is considerable enhanced by 9.26% and 8.27% respectively. During the case-2 shading pattern, both the proposed ACM and HMACM configurations outperformed the TCT and CBM configurations by enhancing the GMP by 33.19%, 25.80%, and 18.51%, 11.94% respectively. During the case-3 shading pattern, the existing CBM configuration yields 1.58% less GMP compared to benchmark TCT. This drawback is rectified by executing the proposed ACM and HMACM configurations. By employing the proposed ACM and HMACM configurations,

the GMP under case-3 is highly enhanced by 19.68%, 18.4%, and 21.6%, 20.3% when compared to the TCT and CBM configurations respectively. The HM configuration also yields higher GMP compared to the TCT and CBM configurations under case-2 and case-3 respectively. The maximum and minimum enhancement in the GMP obtained by the proposed ACM, HM, and HMACM configurations are 33.19%, 25.80% 20.3%, and 12.43%, 0.12%, 8.27% respectively. With the proposed ACM and HMACM configurations, this mismatch power is also reduced significantly. The improved values of performance indices by the proposed configurations validate their superior performance over TCT and CBM configurations as given in Table 2.

During progressive triangular shading

A group of three different cases of progressive triangular shading patterns of case-4 to case-6 as shown in Figure 9 is studied to prove the potency of the proposed configurations.

The corresponding PV characteristics of TCT, CBM, ACM, HM, and HMACM configurations for progressive triangular shading cases are shown in Figure 10. For case-4 shading, all the proposed ACM, HM, HMACM, and CBM configurations enhance the output power by 17.9%, 11.88%, 13.06%, and 17.91% when compared to the conventional TCT configuration. For case-5 shading pattern, the proposed ACM and HMACM configurations effectively enhance the GMP by 26.3% and 28.23% respectively, whereas the CBM configuration yield comparatively less enhancement in output which is only 18.6%. For case-6 shading pattern, the proposed ACM and HMACM configurations efficiently enhance the GMP by 35.25% and 36.85% respectively, whereas the CBM configuration yield only a 23% increase in the output. The proposed ACM and HMACM yield the lowest power mismatch and highest FF compared to both conventional and the existing CBM configurations for case-5 and case-6 shading conditions respectively as observed in Table 2. Hence it is noteworthy to state that the proposed configurations render extremely superior performance during PS conditions.

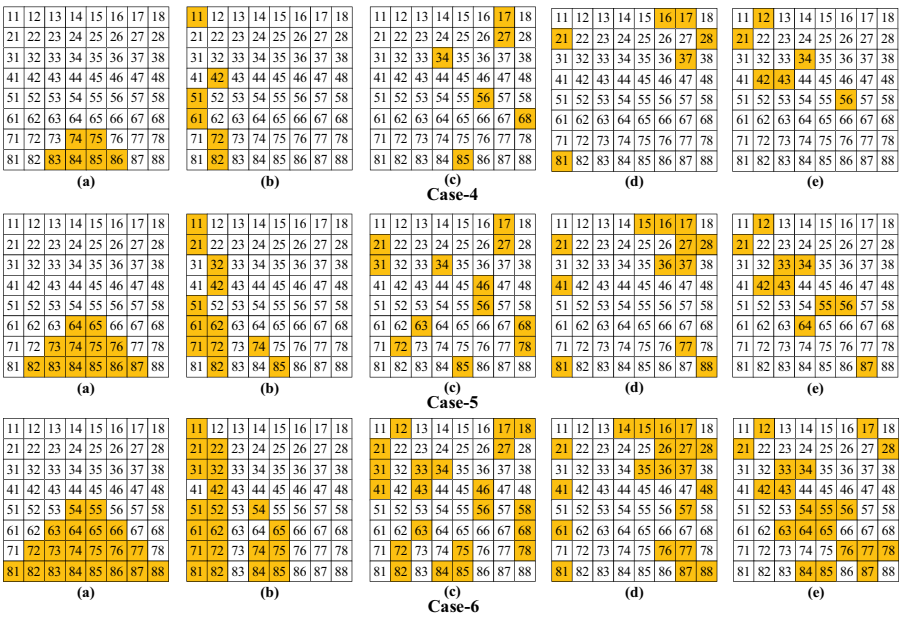

Figure 9. Progressive triangular shading in (a) TCT, shade dispersion with (b) CBM (c) ACM (d) HM (e) HMACM for case-4, case-5 and case-6 respectively.

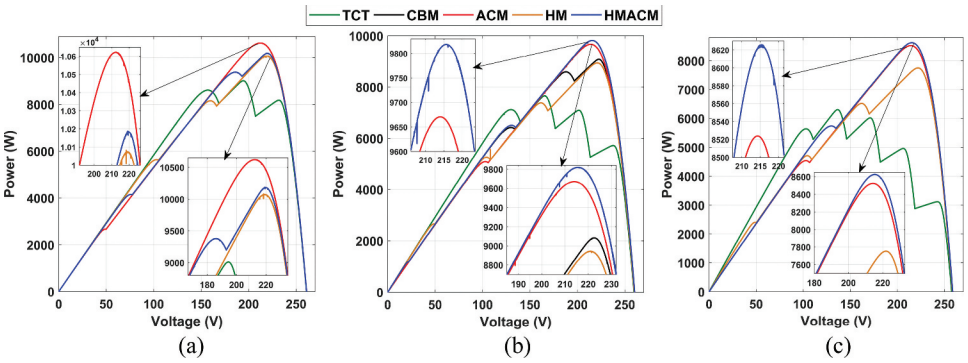

Figure 10. PV characteristics under progressive triangular shading of (a) case-4 (b) case-5 and (c) case-6.

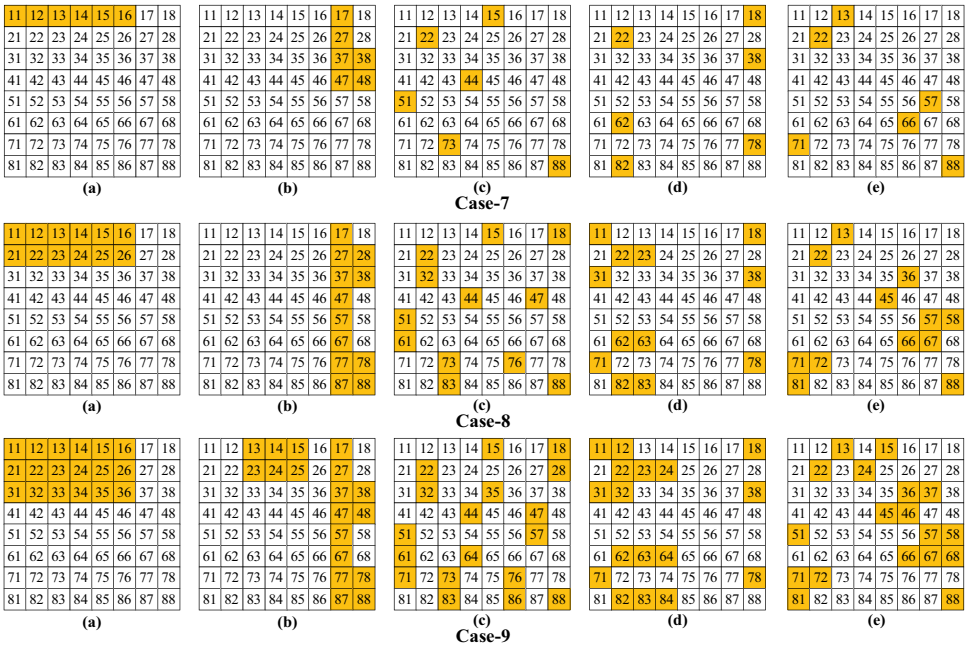

Figure 11. Progressive top-to-bottom shading in (a) TCT, shade dispersion with (b) CBM (c) ACM (d) HM and (e) HMACM for case-7, case-8 and case-9 respectively.

During progressive top-to-bottom shading

Under this type of shading, three distinct cases of progressive top-to-bottom shading patterns of case-7 to case-9 are considered for analysis as shown in Figure 11.

During this shading group of three progressive PS patterns, when compared to both TCT and the existing CBM, all the proposed ACM, HM, and HMACM configurations generate the highest GMP with lesser bypasses and hence obtain much smoother PV characteristics as shown in Figure 12. For case-7 shading pattern, the CBM fails to effectively disperse the shade and thus yield lesser power even compared to TCT. However, by employing the proposed ACM, HM, and HMACM, the GMP is enhanced by 5.24% respectively. For the case-8 shading pattern, all the configurations enhance the output approximately by 12% compared to TCT. For the case-9 shading pattern, the existing CBM enhances the GMP by only 9.88%, whereas the proposed ACM, HM, and HMACM configurations enhance by 22.7%, 18.88%, and 22.72% respectively. Under this shading group, the CBM configuration

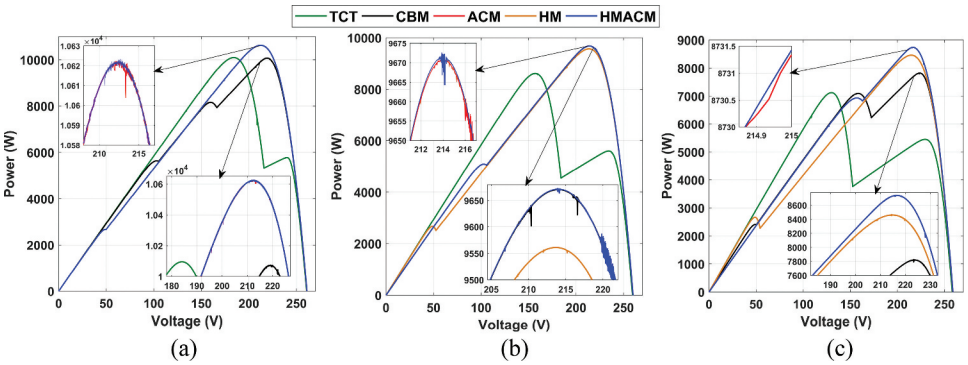

Figure 12. Array PV characteristics under progressive top-to-bottom shading of (a) case-7 (b) case-8 and (c) case-9.

is superior to TCT only in two shading cases, and hence the proposed ACM, HM and HMACM configurations demonstrate their superior and reliable performance over other configurations under all the patterns of top-to-bottom shading group. From Table 2 it is noted that the mismatch power obtained by TCT configuration is 1487 W, 2972.6 W, and 4459.2 W for case-7, case-8 and case-9 respectively. The corresponding mismatch is considerably lowered to 960 W, 1911.3 W, 2842.6 W, and 959 W, 1909.5 W, 2841.3 W by employing the proposed ACM and HMACM configurations.

During progressive diagonal shading

Three distinct cases of diagonal shading patterns which are progressive in nature from case-10 to case-12 are considered as shown in Figure 13.

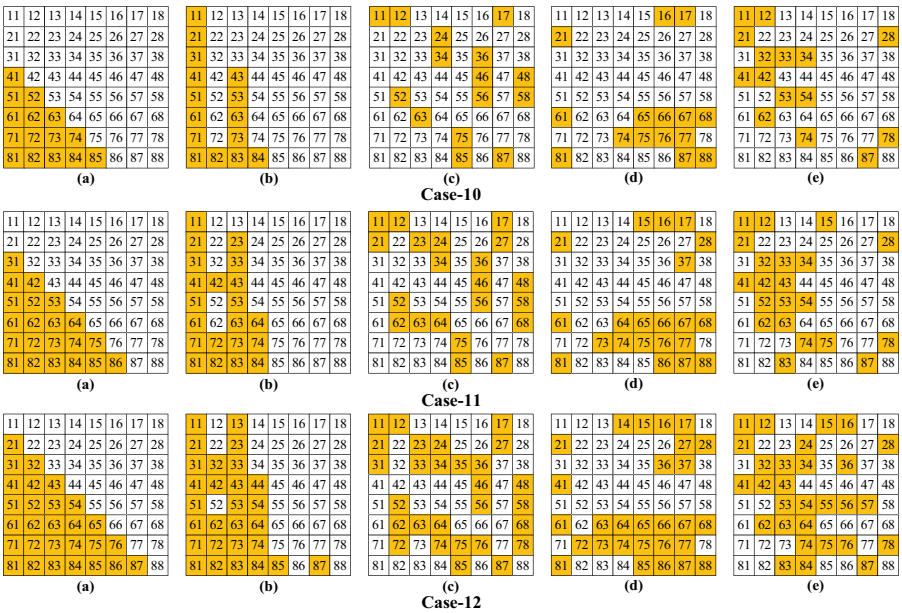

Figure 13. Progressive diagonal shading in (a) TCT, shade dispersion with (b) CBM (c) ACM (d) HM (e) HMACM for case-10, case-11 and case-12 respectively.

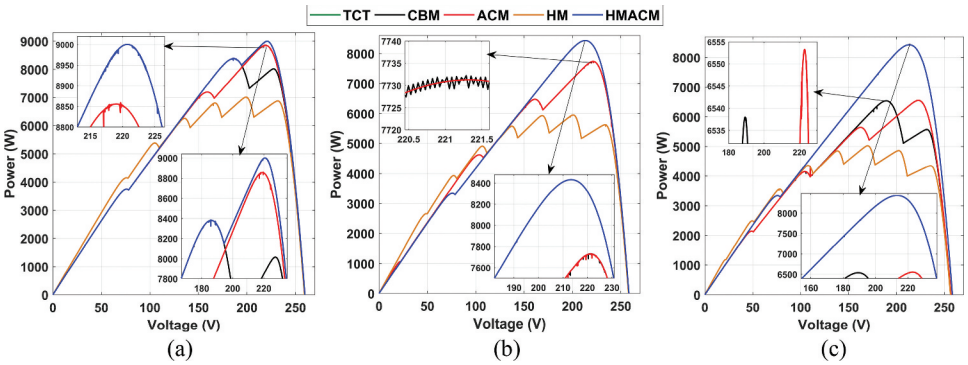

Figure 14. Array PV characteristics under progressive diagonal shadings of (a) case-10 (b) case-11 and (c) case-12.

Table 1. Comparison of GMP obtained by the proposed configurations with TCT and CBM configurations of 8 × 8 PV array under various progressive shading patterns.

	TCT	CBM (Tatabhatla, Agarwal, and Kanumuri 2020)		ACM			HM		HMACM		
Case	GMP (W)	GMP (W)	% more w.r.t TCT	GMP (W)	% more w.r.t TCT	% more w.r.t CBM	GMP (W)	% more w.r.t TCT	GMP (W)	% more w.r.t TCT	% more w.r.t CBM
Under Left-right shading group:											
1	8934.9	9193.8	2.89	10045	12.43	9.26	8944.8	0.12	9953.3	11.40	8.27
2	7122.9	8005.2	12.38	9486.6	33.19	18.51	8606.8	20.84	8960.6	25.80	11.94
3	7122.7	7010.1	− 1.58	8523.9	19.68	21.60	8406.3	18.03	8432.8	18.40	20.30
Under Triangular shading group:											
4	9011.0	10625	17.91	10622	17.88	-	10081	11.88	10187	13.06	-
5	7657.2	9082.1	18.60	9670.7	26.30	6.49	8945.3	16.83	9818.4	28.23	8.11
6	6302.6	7752.7	23.00	8523.9	35.25	9.95	7753.1	23.02	8624.7	36.85	11.25
Under Top-to-bottom shading group:											
7	10095	10074	− 0.21	10622	5.21	5.44	10622	5.23	10623	5.24	5.45
8	8609.4	9670.7	12.32	9670.7	12.33	-	9561	11.06	9672.5	12.35	0.019
9	7122.8	7826.9	9.88	8739.4	22.70	11.66	8467.1	18.88	8740.7	22.72	11.68
Under Diagonal shading group:											
10	7008.3	8381.3	19.59	8858.9	26.41	5.70	7008.2	-	9000.4	28.43	7.392
11	5949.6	7732.2	29.96	7731.2	29.95	-	5949.5	-	8432.8	41.74	9.071
12	5025.3	6538.0	30.10	6553.3	30.41	0.24	5025.3	-	7374.1	46.74	12.79

Under this shading condition, the proposed ACM and HMACM yield the highest GMP with a narrow row current difference thereby exhibiting fewer MPPs. It is noted from the PV characteristics shown in Figure 14 that with the TCT, the number of MPPs is increased from four to six as the diagonal shading increases progressively from case-10 to case-12. However, by employing the proposed ACM and HMACM, the MPPs are reduced to only three and two respectively and there is also no increment in MPPs with the progressive increment in shading concentration. With HMACM, the GMP obtained is improved by 28.43%, 41.74%, 46.74% under case-10, case-11, and case-12 shading patterns respectively. Further, when compared to the CBM, HMACM enhances the GMP by 7.392%, 9.07%, and 12.79% respectively. The GMP obtained for HM and TCT are the same and except for this particular shading group, the proposed HM enhances the output in the range of 11 to 23% for all the other considered shading groups. From case-10 to case 12, the respective mismatch power is greatly reduced to 2581.6 W, 3149.2 W, 4207.9 W, and 2723.1 W, 3850.8 W, 5028.7 W, by employing the proposed HMACM and ACM respectively. The comparison of GMP obtained by various techniques

Table 2. Comparison of mismatch power and fill factor obtained with TCT, CBM, ACM, HM, and HMACM configurations under various progressive shading patterns.

	Mismatch power (W)					Fill Factor				
Case	TCT	CBM	ACM	HM	HMACM	TCT	CBM	ACM	HM	HMACM
Under Left-to-Right shading group:										
1	2647.1	2388.2	1537.0	2637.2	1628.7	0.458	0.471	0.570	0.458	0.510
2	4459.1	3576.8	2095.4	2975.2	2621.4	0.365	0.454	0.539	0.441	0.509
3	4459.3	4571.9	3058.1	3175.7	3149.2	0.365	0.398	0.542	0.431	0.537
Under Triangular shading group:										
4	2571.0	957.0	960.0	1501.0	1395.0	0.462	0.545	0.545	0.517	0.522
5	3924.8	2499.9	1911.3	2636.7	1763.6	0.392	0.471	0.503	0.459	0.511
6	5279.4	3829.3	3058.1	3828.9	2957.3	0.305	0.440	0.471	0.440	0.490
Under Top-to-bottom shading group:										
7	1487.0	1508.0	960.0	960.0	959.0	0.517	0.516	0.545	0.545	0.545
8	2972.6	1911.3	1911.3	2021.0	1909.5	0.441	0.549	0.549	0.490	0.549
9	4459.2	3755.1	2842.6	3114.9	2841.3	0.365	0.441	0.459	0.434	0.471
Under Diagonal shading group:										
10	4573.7	3200.7	2723.1	4573.8	2581.6	0.359	0.476	0.503	0.359	0.511
11	5632.4	3849.8	3850.8	5632.5	3149.2	0.305	0.439	0.439	0.305	0.537
12	6556.7	5044.0	5028.7	6556.7	4207.9	0.257	0.416	0.417	0.257	0.469

under distinct progressive shading conditions is shown in Table 1. It is observed from Fig. 7, 9, 11, and 13, the shade dispersion is very effective with the proposed chaotic map-based ACM and HMACM approaches. However, the existing CBM disperse the shade only in a part of an array.

Validation of proposed techniques for unsymmetrical PV arrays

On contrary to most of the existing static reconfiguration techniques (Dhanalakshmi and Rajasekar 2018; Nasiruddin et al. 2019; Pachauri et al. 2018; Rajani and Ramesh 2021; Rani, Ilango, and Nagamani 2013; Reddy and Yammani 2020; Tatabhatla, Agarwal, and Kanumuri 2020; Varma, Barry, and Jain 2021; Venkateswari and Rajasekar 2020; Yadav, Pachauri, and Chauhan 2016), the proposed ACM, and HMACM can be scalable and compatible with all symmetrical m × m and unsymmetrical m × n PV arrays. The existing CBM (Tatabhatla, Agarwal, and Kanumuri 2020) technique is not compatible with the unsymmetrical arrays. To overcome these setbacks and to demonstrate the compatibility of proposed techniques, a 6.5 kW unsymmetrical 5 × 7 PV array (with nominal voltage and current at P_{max} are 125.4 V and 51.83 A) is tested under distinct groups of progressive shading conditions as shown in Figure 16. Further, their performance has been compared with the conventional SP, TCT, existing OE (Nasiruddin et al. 2019), and OEP (Reddy and Yammani 2020) pattern-based reconfiguration techniques. The Original 5 × 7 matrix and corresponding rearranged matrices obtained by various techniques is shown in Figure 15. When compared to all configurations, the proposed ACM and HMACM effectively disperse the shade uniformly over the entire array mitigating the mismatch and enhancing the output. From the PV characteristics (Fig.17–19) and Table 3, it is noted that the highest GMP is obtained by the proposed techniques. It is noted from Table 3 that the existing OE and OEP techniques despite being effective in some cases offer highly inferior performance under some cases (cases 13–15, 19–20) even compared to the conventional TCT resulting an inconsistent and unreliable performance.

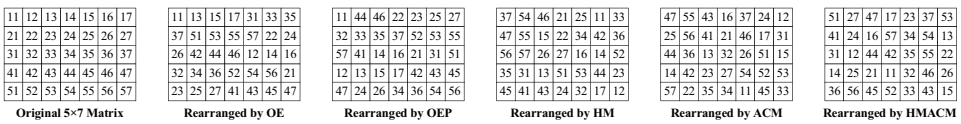

Figure 15. Original 5 × 7 matrix and corresponding rearranged matrices obtained by various techniques.

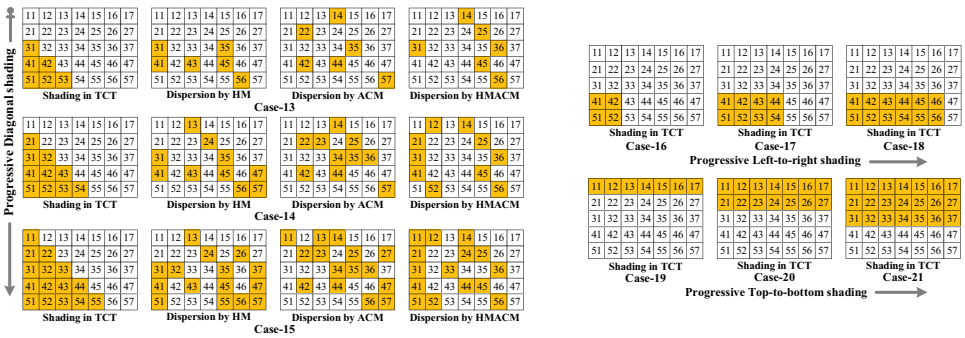

Figure 16. Distinct progressive shading cases for a 5 × 7 PV array.

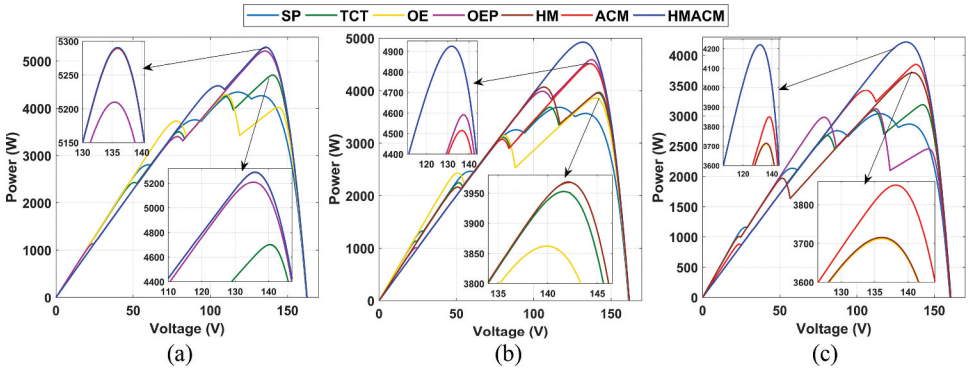

Figure 17. PV characteristics under progressive diagonal shadings of (a) case-13 (b) case-14 and (c) case-15.

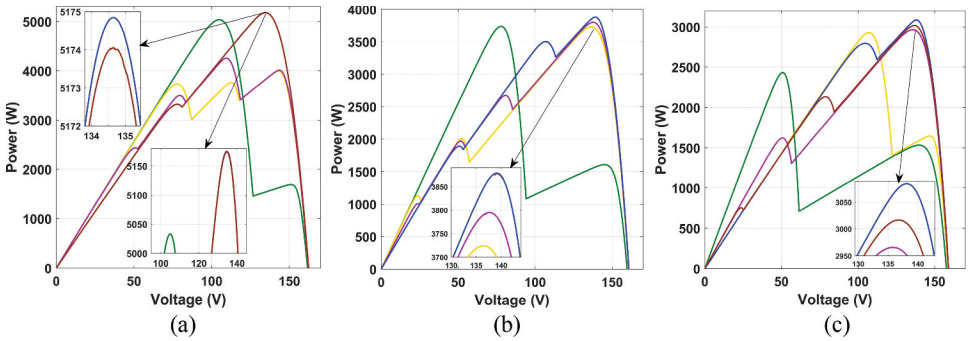

Figure 18. PV characteristics under progressive left-to-right shadings of (a) case-16 (b) case-17 and (c) case-18.

Experimental validation of proposed techniques

A laboratory experimental setup is developed to justify the obtained simulation results of various configurations as shown in Figure 20. Sixteen 3-Watt polycrystalline PV panels are connected in a 4 × 4 PV array of TCT, CBM, OE, OEP, ACM, and HMACM-based configurations using the banana plug connectors and interconnection wires as shown in Figure 20. The output terminals of the array are connected to a variable sliding rheostat (300 Ω and 1.5 Ampere). The rheostat is adjusted to set at a fixed point for extracting maximum power from the array. Two SM7023A scientific digital multimeters are used to measure the array voltage and the current flowing through rheostat. Four artificial lighting sources (A1 to A4) constituting multiple halogen bulbs emulating the sun's irradiation are

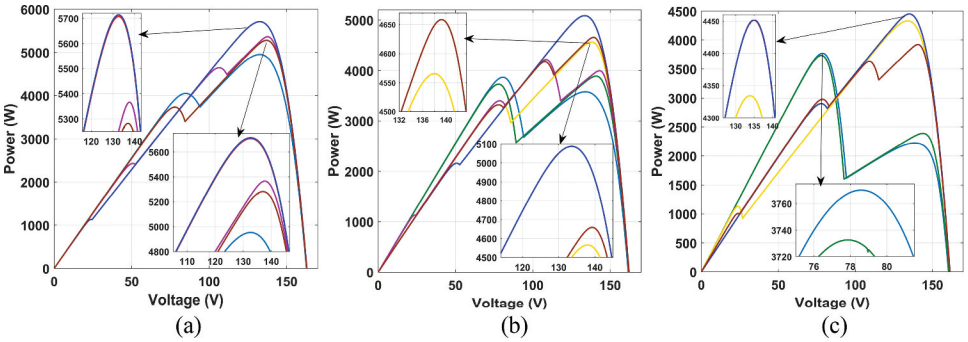

Figure 19. PV characteristics under progressive top-to-bottom shadings of (a) case-19 (b) case-20 and (c) case-21.

Table 3. Comparison of GMP obtained by various configurations of unsymmetrical 5 × 7 PV array.

	GMP (in Watt)											
Case	SP	TCT	OE (Nasiruddin et al. 2019)	% gain	OEP (Reddy and Yammani 2020)	% gain	HM	% gain	ACM	% gain	HMACM	% gain
Under Progressive Diagonal shading group												
13	4340.0	4700.9	4292.6	−8.69	5210.0	10.83	5290.7	12.55	5289.5	12.52	5290.7	12.55
14	3685.4	3952.8	3862.3	−2.29	4591.8	16.17	4073.2	3.05	4514.2	14.20	4924.9	24.59
15	3037.2	3183.5	3712.1	16.6	3116.4	−2.11	3712.1	16.6	3850.5	20.95	4219.8	32.55
Under Progressive Left-to-Right shading group												
16	4952.8	5282.6	5282.6	0	5366.4	1.59	5282.6	**0**	5707.1	8.04	5707.1	8.04
17	3869.6	3891.2	4565.5	17.33	4216.6	8.36	4658.4	19.72	4658.4	19.72	5087.8	30.75
18	3770.2	3732.7	4334.3	16.12	3923.1	5.10	3923.1	5.10	4451.5	19.26	4452.0	19.27
Under Progressive Top-to-bottom shading group												
19	5033.1	5033.1	3995.1	−20.62	4254.5	−15.47	5174.1	2.80	5174.1	2.80	5174.8	2.82
20	3732.6	3732.6	3724.0	−0.23	3794.7	1.66	3878.2	3.92	3878.8	3.92	3878.8	3.92
21	2432.1	2432.1	2928.1	20.39	2965.6	21.94	3016.5	24.03	3016.5	24.03	3081.1	26.68

utilized to emit the lighting to energize the PV panels. Each lighting source energizes four PV panels as shown in the experimental test bench. A portable TENMARS TM-206 digital solar power meter is employed to measure the irradiation level (in W/m^2) generated by the artificial light source. An AEC HTD8813C infrared thermometer gun is employed to measure the operating temperature of panels. During unshaded conditions, the panels receive the irradiation of 305 W/m^2 approximately by each lighting source. As shown in Figure 20, the artificial shading conditions are created by thin transparent sheets that mitigate the irradiation reaching the panels.

The shaded panels receive the irradiation of nearly 160 W/m^2 and the temperature of the panels is found to be 33°C. The PV array is connected in various configurations and tested under three distinct groups of dynamically moving shade over the array in top-to-bottom, diagonal, and left-to-right directions as shown in Figure 21. Besides, a progressive diagonally moving shade is also considered. The output obtained by various configurations under these shading groups is given in Figure 22. It is noted that the proposed image encryption-based techniques exhibit consistently superior shade dispersion outperforming all other existing configurations. The existing CBM and OEP generate considerably low power compared to conventional TCT under case-25 to case-27 due to their poor shade dispersion under certain shading conditions.

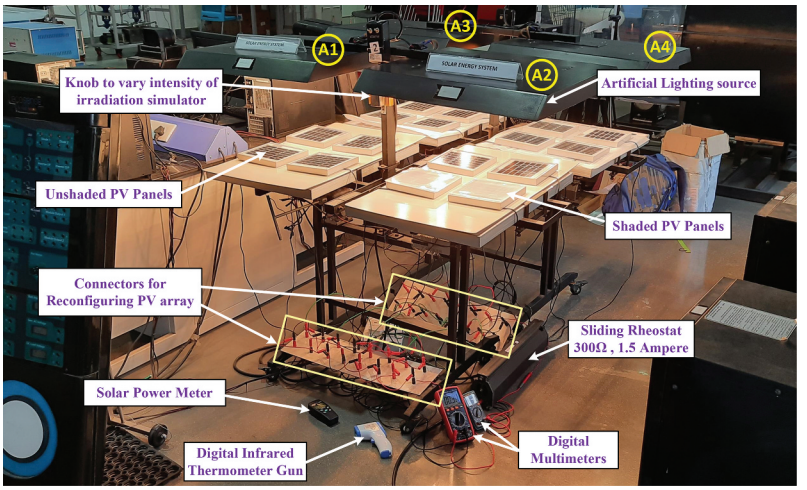

Figure 20. Laboratory experimental setup of a 4 × 4 PV array reconfiguration system.

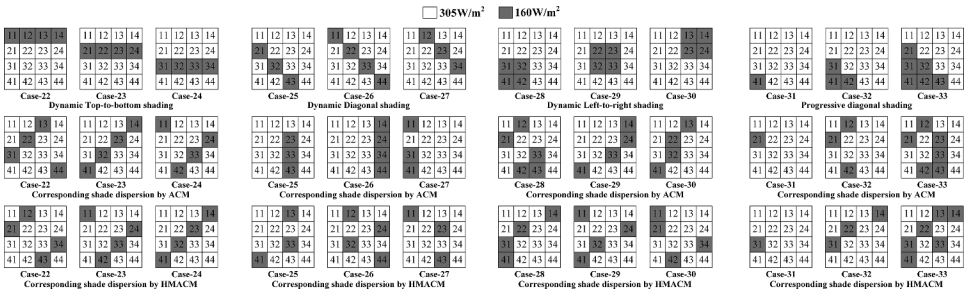

Figure 21. Distinct shading cases and respective shade dispersion by ACM and HMACM for a 4 × 4 PV array.

Qualitative comparative summary with other state-of-art techniques

The qualitative comparative performance summary of the proposed techniques with other state-of-art techniques is presented in Figure 23.

- The proposed configurations are economically and practically feasible as they are one-time arrangements and don't require sensors, switches, relays, controllers, switching matrix, driver circuits, an infrared thermal imaging camera, monitoring systems, etc., for dispersing the shade which is highly demanded by the existing dynamic techniques (Ajmal et al. 2021; Karakose et al. 2016; Pachauri et al. 2019; Yadav et al. 2022). All these factors result in higher installation and operational costs for dynamic configurations significantly increasing the payback period. However, a lowest payback period can be achieved with the proposed configurations.
- Unlike, metaheuristic optimization-based techniques (Babu et al. 2018; Babu, Yousri, and Balasubramanian 2020; Deshkar et al. 2015; Yousri, Allam, and Eteiba 2020), the proposed techniques don't involve complicated algorithms, complex search mechanisms, large computations, convergence issues, tuning parameter difficulties, etc for reconfiguring the PV array. Further, they use weighted sum approach in solving a multi-objective optimization problem

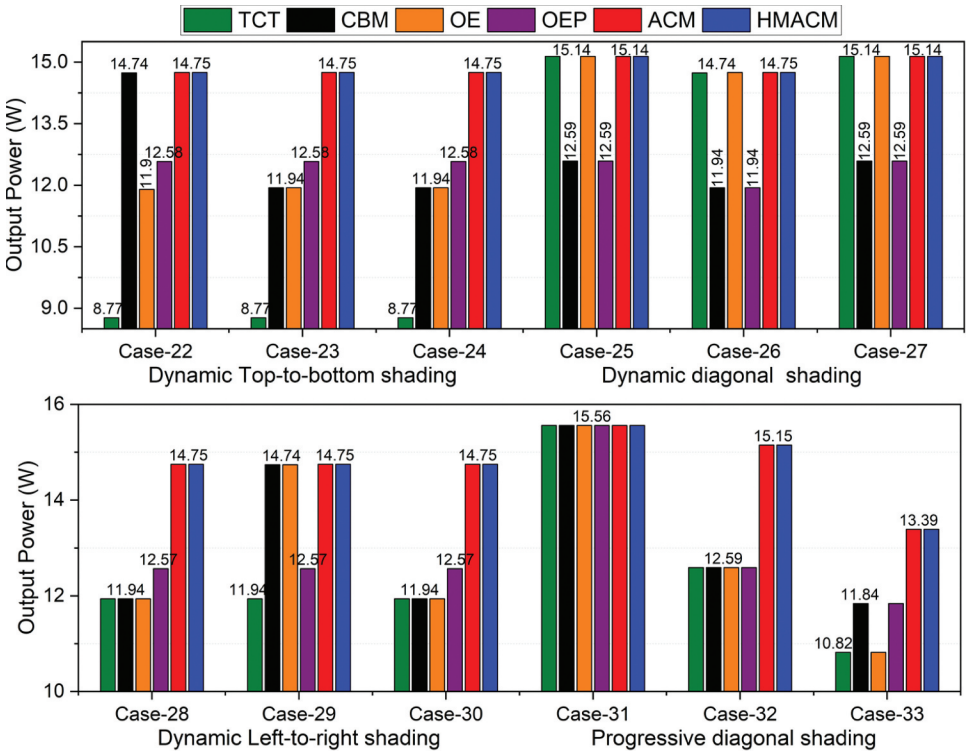

Figure 22. Experimental test results of various configurations under dynamic and progressive shading conditions.

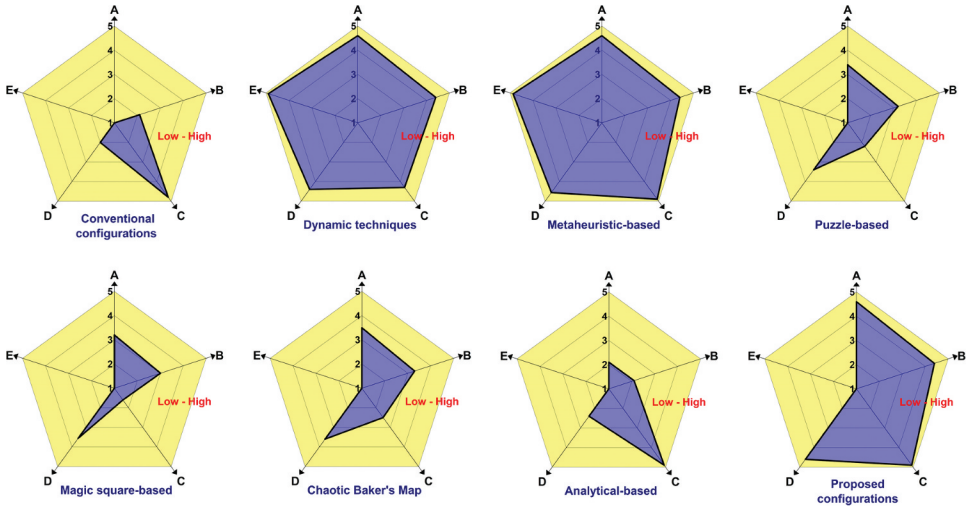

Figure 23. Radar chart describing performance comparison of proposed techniques with state of art techniques. (a) shade dispersion capability (b) GMP Obtained, (c) Compatibility, (d) Power Enhancement, (e) Switches and sensors requirement

for maximizing the power and mitigating the mismatch loss. Nevertheless, the main drawback/challenge associated with the weighted sum approach is selecting the optimal weights. Improper selection of these weights affects the output significantly.

- Most of the puzzle-based techniques (Dhanalakshmi and Rajasekar 2018; Pachauri et al. 2018; Rajani and Ramesh 2021; Rani, Ilango, and Nagamani 2013; Venkateswari and Rajasekar 2020; Yadav, Pachauri, and Chauhan 2016) disperse the shade indiscriminately and are applied to certain array sizes and hence cannot be scalable and generalized. However, the proposed techniques are compatible with all array sizes and disperse the shade evenly by reducing the amount of shading in a particular row of the array.
- The scalability of recently proposed Magic-square-based topologies (Varma, Barry, and Jain 2021; Venkateswari and Rajasekar 2020) is highly limited to few array sizes and further exhibits unreliable shade dispersion in some cases.
- In contrast to CBM (Tatabhatla, Agarwal, and Kanumuri 2020), the proposed techniques offer a superior and reliable performance with uniform shade dispersion over the entire array. Further, the CBM technique cannot be applicable to all symmetrical and unsymmetrical array sizes.
- On contrary to the analytical approaches such as OE (Nasiruddin et al. 2019) and OEP (Reddy and Yammani 2020), the proposed technique yields smoother array characteristics with reduced multiple power peaks lowering the burden on MPPT controllers in differentiating the global and local MPPs.

Hence, from the extensive comparative analysis, it is remarked that proposed image encryption-based ACM and HMACM techniques offer a more suitable solution for shading compared to many other state-of-art techniques.

Conclusions and future scope

In this paper, two highly efficient chaotic approaches-Arnold's Cat Map and Henon Map are employed to reconfigure the PV array. The proposed approaches are evaluated for various symmetrical 8×8, 4×4, and unsymmetrical 5×7 PV arrays. Their performance has been compared with conventional SP, TCT, CBM, OE, and OEP configurations under 33 cases of distinct progressive and dynamic shading groups. In some cases, the existing CBM, OE, and OEP reconfiguration techniques exhibit inferior performance even compared to conventional TCT offering an inconsistent and unreliable solution. Whereas, the proposed chaotic map-based ACM and HMACM approaches yield consistently superior performance over the existing configurations under all shading cases. By employing respective ACM and HMACM, the output enhancement is found to be in the range of (5.21 to 35.25)% and (5.24 to 46.74)% for an 8×8 PV array; (2.80 to 24.03)% and (2.82 to 32.55)% for a 5×7 PV array. It is noted that the enhancement with HMACM is slightly more compared to ACM in many cases as it uses the dual-stage chaotic mapping which disperses the shade much more effectively. Additionally, the proposed configurations yield the lowest mismatch and highest FF. Further, the proposed techniques are experimentally validated for a 4×4 PV array under distinct shading conditions.

Hence, it is concluded that the superior and reliable performance of the proposed chaotic approach-based reconfiguration techniques is the need of the moment to enhance the output and mitigate the mismatch losses during partial shading conditions. In the future, these techniques can also be effectively implemented in PV array dynamic reconfiguration strategies for finding the optimal switching matrix pattern. Executing this will evade the setbacks associated with metaheuristic and other optimization algorithms. Besides, an MPPT incorporated chaotic approach-based reconfiguration system for GMP tracking can be further investigated for rooftop and large-rated commercial PV farms.

Disclosure statement

No potential conflict of interest was reported by the author(s).

ORCID

Rayappa David Amar Raj http://orcid.org/0000-0002-5888-5513
Kanasottu Anil Naik http://orcid.org/0000-0002-3321-5097

Data availability statement

Data sharing is not applicable to this article as no new data were created or analyzed in this study.

References

Ahmad, R., A. M. Sher, U. T. Shami, S. Olalekan, and S. Olalekan. 2017. An analytical approach to study partial shading effects on PV array supported by literature. *Renew and Sustain Ener. Rev* 74:721–32. doi:10.1016/j.rser.2017.02.078.

Ajmal, A. M., V. K. Ramachandaramurthy, A. Naderipour, and J. B. Ekanayake. 2021. Comparative analysis of two-step GA-based PV array reconfiguration technique and other reconfiguration techniques. *Energy Conversion and Management* 230:113806. doi:10.1016/j.enconman.2020.113806.

Babu, T. S., J. P. Ram, T. Dragičević, M. Miyatake, F. Blaabjerg, and N. Rajasekar. 2018. Particle swarm optimization based solar PV array reconfiguration of the maximum power extraction under partial shading conditions. *IEEE Transactions on Sustainable Energy* 9 (1):74–85. doi:10.1109/TSTE.2017.2714905.

Babu, T. S., D. Yousri, and K. Balasubramanian. 2020. Photovoltaic array reconfiguration system for maximizing the harvested power using population-based algorithms. *IEEE Access* 8:109608–24. doi:10.1109/ACCESS.2020.3000988.

Belhachat, F., and C. Larbes. 2021. PV array reconfiguration techniques for maximum power optimization under partial shading conditions: A review. *Solar Energy* 230:558–82. doi:10.1016/j.solener.2021.09.089.

Belhaouas, N., M. S. A. Cheikh, P. Agathoklis, M. R. Oularbi, B. Amrouche, K. Sedraoui, and N. Djilali. 2017. PV array power output maximization under partial shading using new shifted PV array arrangements. *Applied Energy* 187:326–37. doi:10.1016/j.apenergy.2016.11.038.

Celikel, R., M. Yilmaz, and A. Gundogdu. 2022. A voltage scanning-based MPPT method for PV power systems under complex partial shading conditions. *Renewable Energy* 184:361–73. doi:10.1016/j.renene.2021.11.098.

Deshkar, S. N., S. B. Dhale, J. S. Mukherjee, T. S. Babu, and N. Rajasekar. 2015. Solar PV array reconfiguration under partial shading conditions for maximum power extraction using genetic algorithm. *Renewable and Sustainable Energy Reviews* 43:102–10. doi:10.1016/j.rser.2014.10.098.

Dhanalakshmi, B., and N. Rajasekar. 2018. Dominance square based array reconfiguration scheme for power loss reduction in solar PhotoVoltaic (PV) systems. *Energy Conversion and Management* 156:84–102. doi:10.1016/j.enconman.2017.10.080.

Horoufiany, M., and R. Ghandehari. 2018. Optimization of the Sudoku based reconfiguration technique for PV arrays power enhancement under mutual shading conditions. *Solar Energy* 159:1037–46. doi:10.1016/j.solener.2017.05.059.

Karakose, M., M. Baygin, K. Murat, N. Baygin, and E. Akin. 2016. fuzzy based reconfiguration method using intelligent partial shadow detection in PV arrays. *International Journal of Computational Intelligence Systems* 9 (2):202–12.

Li, C., K. Tan, B. Feng, and J. Lu. 2022. The graph structure of the generalized discrete arnold's cat map. *IEEE Transactions on Computers* 71 (2):364–77. doi:10.1109/TC.2021.3051387.

Mellit, A., and S. Kalogirou. 2021. Artificial intelligence and internet of things to improve efficacy of diagnosis and remote sensing of solar photovoltaic systems: Challenges, recommendations and future directions. *Renewable and Sustainable Energy Reviews* 143:110889. doi:10.1016/j.rser.2021.110889.

Nasiruddin, I., S. Khatoon, M. F. Jalil, and R. C. Bansal. 2019. Shade diffusion of partial shaded PV array by using odd-even structure. *Solar Energy* 181:519–29. doi:10.1016/j.solener.2019.01.076.

Ndi, F. E., S. N. Perabi, S. E. Ndjakomo, G. O. Abessolo, and G. M. Mengata. 2021. Estimation of single-diode and two diode solar cell parameters by equilibrium optimizer method. *Energy Reports* 7:4761–68. doi:10.1016/j.egyr.2021.07.025.

Pachauri, R., R. Singh, A. Gehlot, R. Samakaria, and S. Choudhury. 2019. Experimental analysis to extract maximum power from PV array reconfiguration under partial shading conditions. *Engineering Science and Technology, an International Journal* 22 (1):109–30. doi:10.1016/j.jestch.2017.11.013.

Pachauri, R., A. S. Yadav, Y. K. Chauhan, A. Sharma, and V. Kumar. 2018. Shade dispersion-based photovoltaic array configurations for performance enhancement under partial shading conditions. *International Transactions on Electrical Energy Systems* 28 (7):28. doi:10.1002/etep.2556.

Peng, Y., K. Sun, and S. He. 2020. A discrete memristor model and its application in Hénon map. *Chaos, Solitons & Fractals* 137:109873. doi:10.1016/j.chaos.2020.109873.

Pillai, D. S., N. Rajasekar, J. P. Ram, and V. K. Chinnaiyan. 2018. Design and testing of two phase array reconfiguration procedure for maximizing power in solar PV systems under partial shade conditions (PSC. *Energy Conversion and Management* 178:92–110. doi:10.1016/j.enconman.2018.10.020.

Ping, P., Y. Mao, X. Lv, F. Xu, and G. Xu. 2015. An image scrambling algorithm using discrete Henon map. IEEE International Conference on Information and Automation Lijiang, China, pp.429–32.
Rahman, M. M., I. Khan, and K. Alameh. 2021. Potential measurement techniques for photovoltaic module failure diagnosis: A review. *Renewable and Sustainable Energy Reviews* 151:111532. doi:10.1016/j.rser.2021.111532.
Rajani, K., and T. Ramesh. 2021. Maximum power enhancement under partial shadings using a modified Sudoku reconfiguration. *CSEE Journal of Power and Energy Systems* 7 (6):1187–201.
Rakesh, N., S. Subramaniam, B. Natarajan, and M. Udugula. 2022. A non-puzzle based interconnection scheme for energy savings and income generation from partially shaded photovoltaic modules. *Energy Sources* Part A: Recovery, Utilization, and Environmental Effects, 1–19. doi:10.1080/15567036.2022.2029973.
Rani, B. I., G. S. Ilango, and C. Nagamani. 2013. Enhanced power generation from PV array under partial shading conditions by shade dispersion using Su Do Ku configuration. *IEEE Transactions on Sustainable Energy* 4 (3):594–601. doi:10.1109/TSTE.2012.2230033.
Reddy, S. S., and C. Yammani. 2020. Odd-even-prime pattern for PV array to increase power output under partial shading conditions. *Energy* 213:118780. doi:10.1016/j.energy.2020.118780.
Rezazadeh, S., A. Moradzadeh, K. Pourhossein, B. Mohammadi-Ivatloo, and F. P. G. Márquez. 2022. Photovoltaic array reconfiguration under partial shading conditions for maximum power extraction via knight's tour technique. *Journal of Ambient Intelligence and Humanized Computing*. doi:10.1007/s12652-022-03723-1.
Satpathy, P. R., T. S. Babu, A. Mahmoud, R. Sharma, and B. Nastasi. 2021. A TCT-SC hybridized voltage equalizer for partial shading mitigation in PV arrays. *IEEE Transactions on Sustainable Energy* 12 (4):2268–81. doi:10.1109/TSTE.2021.3088687.
Satpathy, P. R., and R. Sharma. 2018. Power loss reduction in partially shaded PV arrays by a static SDP technique. *Energy* 156:569–85. doi:10.1016/j.energy.2018.05.131.
Satpathy, P. R., and R. Sharma. 2019. Power and mismatch losses mitigation by a fixed electrical reconfiguration technique for partially shaded photovoltaic arrays. *Energy Conversion and Management* 192:52–70. doi:10.1016/j.enconman.2019.04.039.
Satpathy, P. R., R. Sharma, and S. Dash. 2019. An efficient SD-PAR technique for maximum power generation from modules of partially shaded PV arrays. *Energy* 175:182–94. doi:10.1016/j.energy.2019.03.078.
Satpathy, P. R., R. Sharma, and S. Jena. 2017. A shade dispersion interconnection scheme for partially shaded modules in a solar PV array network. *Energy* 139:350–65. doi:10.1016/j.energy.2017.07.161.
Shahna, K. U., and A. Mohamed. 2020. A novel image encryption scheme using both pixel level and bit level permutation with chaotic map. *Applied Soft Computing* 90:106162. doi:10.1016/j.asoc.2020.106162.
Smith, R. M., M. Matam, and H. Seigneur. 2021. Mismatch losses in a PV system due to shortened strings. *Energy Conversion and Management* 250:114891. doi:10.1016/j.enconman.2021.114891.
Tatabhatla, V. M. R., A. Agarwal, and T. Kanumuri. 2020. A generalized chaotic baker map configuration for reducing the power loss under shading conditions. *Electrical Engineering* 102:2227–44. doi:10.1007/s00202-020-01016-4.
Varma, G. H. K., V. R. Barry, and R. K. Jain. 2021. a novel magic square based physical reconfiguration for power enhancement in larger size photovoltaic array. *IETE Journal Of Research*. https://doi.org/10.1080/03772063.2021.1944333
Venkateswari, R., and N. Rajasekar. 2020. Power enhancement of PV system via physical array reconfiguration based Lo Shu technique. *Energy Conversion and Management* 215:112885. doi:10.1016/j.enconman.2020.112885.
Yadav, A. S., R. K. Pachauri, and Y. K. Chauhan. 2016. Comprehensive investigation of PV arrays with puzzle shade dispersion for improved performance. *Solar Energy* 129:256–85. doi:10.1016/j.solener.2016.01.056.
Yadav, V. K., A. Yadav, R. Yadav, A. Mittal, N. H. Wazir, S. Gupta, R. K. Pachauri, and S. Ghosh. 2022. A novel reconfiguration technique for improvement of PV reliability. *Renewable Energy* 182:508–20. doi:10.1016/j.renene.2021.10.043.
Yousri, D., D. Allam, and M. B. Eteiba. 2020. Optimal photovoltaic array reconfiguration for alleviating the partial shading influence based on a modified Harris hawks optimizer. *Energy Conversion and Management* 206:112470. doi:10.1016/j.enconman.2020.112470.